JACS
JOURNAL OF THE AMERICAN CHEMICAL SOCIETY
pubs.acs.org/JACS
Article

Synthesis and Crystallographic Characterization of a Reduced Bimetallic Yttrium *ansa*-Metallocene Hydride Complex, [K(crypt)][(μ-Cp^{An})Y(μ-H)]$_2$ (Cp^{An} = $Me_2Si[C_5H_3(SiMe_3)$-3]$_2$), with a 3.4 Å Yttrium−Yttrium Distance

Justin C. Wedal,[▽] Lauren M. Anderson-Sanchez,[▽] Megan T. Dumas, Colin A. Gould, María J. Beltrán-Leiva, Cristian Celis-Barros, Dayán Páez-Hernández, Joseph W. Ziller, Jeffrey R. Long, and William J. Evans*

Cite This: *J. Am. Chem. Soc.* 2023, 145, 10730−10742

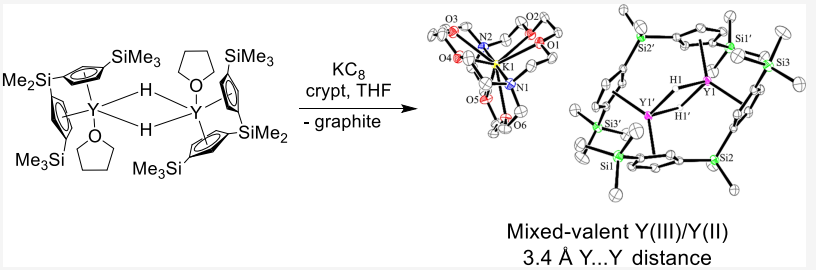

ABSTRACT: The reduction of a bimetallic yttrium *ansa*-metallocene hydride was examined to explore the possible formation of Y−Y bonds with 4d^1 Y(II) ions. The precursor [Cp^{An}Y(μ-H)(THF)]$_2$ (Cp^{An} = $Me_2Si[C_5H_3(SiMe_3)$-3]$_2$) was synthesized by hydrogenolysis of the allyl complex Cp^{An}Y(η^3-C_3H_5)(THF), which was prepared from $(C_3H_5)MgCl$ and [Cp^{An}Y(μ-Cl)]$_2$. Treatment of [Cp^{An}Y(μ-H)(THF)]$_2$ with excess KC_8 in the presence of one equivalent of 2.2.2-cryptand (crypt) generates an intensely colored red-brown product crystallographically identified as [K(crypt)][(μ-Cp^{An})Y(μ-H)]$_2$. The two rings of each Cp^{An} ligand in the reduced anion [(μ-Cp^{An})Y(μ-H)]$_2^{1-}$ are attached to two yttrium centers in a "flyover" configuration. The 3.3992(6) and 3.4022(7) Å Y···Y distances between the equivalent metal centers within two crystallographically independent complexes are the shortest Y···Y distances observed to date. Ultraviolet−visible (UV−visible)/near infrared (IR) and electron paramagnetic resonance (EPR) spectroscopy support the presence of Y(II), and theoretical analysis describes the singly occupied molecular orbital (SOMO) as an Y−Y bonding orbital composed of metal 4d orbitals mixed with metallocene ligand orbitals. A dysprosium analogue, [K(18-crown-6)(THF)$_2$][(μ-Cp^{An})Dy(μ-H)]$_2$, was also synthesized, crystallographically characterized, and studied by variable temperature magnetic susceptibility. The magnetic data are best modeled with the presence of one 4f^9 Dy(III) center and one 4f^9(5d$_{z^2}$)^1 Dy(II) center with no coupling between them. CASSCF calculations are consistent with magnetic measurements supporting the absence of coupling between the Dy centers.

INTRODUCTION

The discovery that the +2 oxidation state was available in crystallographically characterizable complexes not only for Eu,[1−3] Yb,[4−6] Sm,[7−9] Tm,[10−12] Dy,[13−15] and Nd,[16−19] but also for La,[20] Ce,[20] Pr,[21] Gd,[21] Tb,[21] Ho,[22] Er,[22] and Lu[21] as well as Y[23] opened up new opportunities in rare-earth metal reduction chemistry.[24−26] The extensive chemistry previously found for the initial six Ln(II) ions can now be extended to all of the metals in the series, and the new Ln(II) ions have been found to be stronger reductants.[27] Interestingly, the structural, spectroscopic, and magnetic data, together with theoretical calculations for La, Ce, Pr, Gd, Tb, Ho, Er, and Lu, indicated that these lanthanides formed 4f^{n}5d^1 Ln(II) ions by reduction of 4f^n Ln(III) ions rather than the traditional 4f^{n+1} Ln(II) ions of Eu, Yb, Sm, Tm, Dy, and Nd.[9−19,28−30] The data for new Y(II) complexes were consistent with 4d^1 ions.[23] The new complexes initially were isolated and crystallographically characterized in tris(cyclopentadienyl) ligand environments involving $C_5H_4SiMe_3$ (Cp′) and $C_5H_3(SiMe_3)_2$ (Cp″), as shown in eq 1.[20−23,28,30]

Received: February 7, 2023
Published: May 3, 2023

https://doi.org/10.1021/jacs.3c01405
J. Am. Chem. Soc. 2023, 145, 10730−10742

Scheme 1. Synthetic Route to $[K(crypt)][(\mu\text{-}Cp^{An})Y(\mu\text{-}H)]_2$, 4

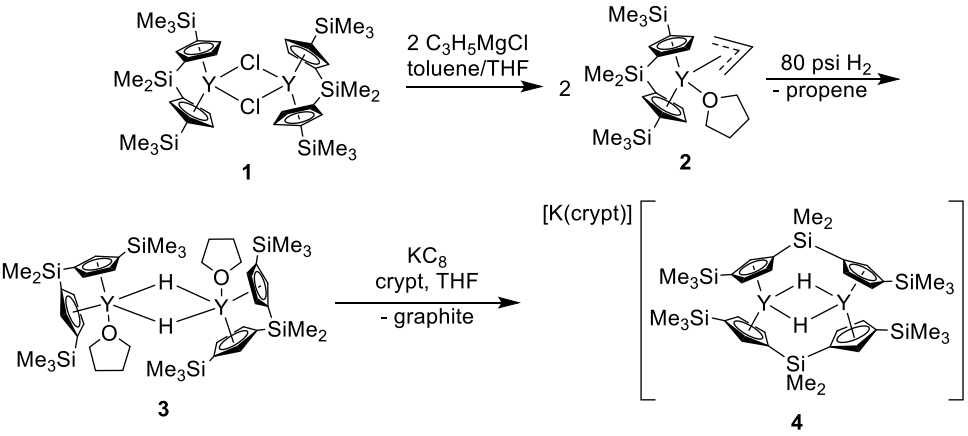

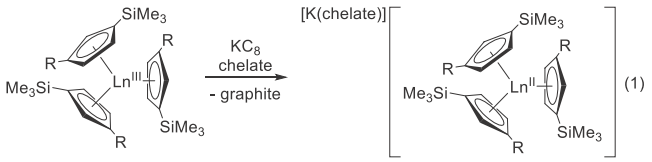

R = H; M = Y, La, Ce, Pr, Nd, Gd, Tb, Dy, Ho, Er, Lu
R = $SiMe_3$; M = La, Ce, Pr
chelate = 18-crown-6 or 2.2.2-cryptand

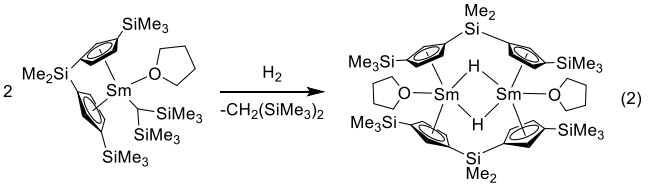

The existence of Ln(II) ions with $4f^n5d^1$ electron configurations raises the possibility of synthesizing bimetallic complexes with metal−metal bonds. Molecular complexes containing bonds between two lanthanide ions have been elusive due to the limited radial extension of the 4f orbitals,[26,31−33] and Y−Y bonds have not been possible with Y(III) because it is a $4d^0$ ion. Metal−metal bonding occurs in the solid state, and bonds between rare-earth metals have been reported within the special environment of fullerenes.[34−41]

Previously, density functional theory (DFT) calculations performed on bridged bimetallic yttrium complexes such as $[Cp'_2Y(\mu\text{-}Cl)]_2$ and $[Cp'_2Y(\mu\text{-}H)(THF)]_2$ suggested that reduction of these species could possibly lead to Y−Y bonds.[42] The bridging hydride and methyl complexes were of special interest since these ligands are involved in electron-deficient three-center two-electron bonding involving a molecular orbital derived from two metal orbitals and a ligand orbital from hydrogen or a methyl group, respectively.[43,44]

To pursue the possibility of generating molecular species containing Y−Y bonds, potassium graphite reductions of $[Cp'_2Y(\mu\text{-}Cl)]_2$,[42] $[Cp'_2Y(\mu\text{-}CH_3)]_2$,[45] and $[Cp'_2Y(\mu\text{-}H)(THF)]_2$[42] were carried out. Dark-colored solutions were generated, which suggested the formation of yttrium in the +2 oxidation state. Both ultraviolet−visible (UV−visible) data and electron paramagnetic resonance (EPR) spectra suggested Y(II) was present, but crystallographic evidence was not obtained for these complexes.[42,45] In the case of the $[Cp'_2Y(\mu\text{-}H)(THF)]_2$ reduction reactions, the only product identified by X-ray crystallography was the Y(III) trimetallic tetrahydride, $[K(crypt)]\{[Cp'_2Y(\mu\text{-}H)]_3(\mu_3\text{-}H)\}$ (crypt = 2.2.2-cryptand).[42]

It was hypothesized that by using the chelating *ansa*-cyclopentadienyl ligand $Me_2Si[C_5H_3(SiMe_3\text{-}3)]_2$, Cp^{An}, the ligand rearrangements which form the polymetallic species could be inhibited. A bimetallic Cp^{An} hydride complex of Sm had been synthesized and crystallographically characterized in 2000, eq 2.[46] In this complex, the Cp^{An} ligands bridge across the two samarium ions in a structure referred to as a "flyover" complex, eq 2.[46] Such a bonding mode would not be expected to favor a trimetallic species, as was observed in the reduction of $[Cp'_2Y(\mu\text{-}H)]_2$, which formed $[K(2.2.2\text{-cryptand})]\{[Cp'_2Y(\mu\text{-}H)]_3(\mu_3\text{-}H)\}$. Since reduction of Sm(III) forms a "traditional" $4f^6$ Sm(II) ion, analogues of the hydride in eq 2 with metals that form $4f^n5d^1$ Ln(II) ions or $4d^1$ Y(II) ions were needed. The synthesis of the yttrium analogue was pursued for reduction studies because ^{89}Y has a 100% naturally abundant $I = 1/2$ nucleus that could be exploited for characterization by EPR spectroscopy. Here, we report the synthesis and crystal structure of a reduced bimetallic yttrium hydride complex and the dysprosium analogue. UV−visible and EPR spectroscopy as well as magnetic characterization support the presence of Ln(II) species. While this work was in progress, the use of $4d^1$ and $4f^n5d^1$ electron configurations to form Ln−Ln bonds has been reported in a mono-cyclopentadienyl iodide bridged bimetallic system, $[(C_5{}^iPr_5)Ln]_2(\mu\text{-}I)_3$ (Ln = Y, Gd, Tb, Dy).[47,48]

RESULTS

Synthesis of $[Cp^{An}Y(\mu\text{-}H)(THF)]_2$. The synthesis of a bimetallic, bridging hydride complex, $[Cp^{An}Y(\mu\text{-}H)(THF)]_2$, which was desired for reduction studies, could be accomplished via hydrogenation of an yttrium alkyl complex, which in turn could be synthesized via salt metathesis using an yttrium halide species. The necessary chloride precursor $[Cp^{An}Y(\mu\text{-}Cl)]_2$, **1**, was previously reported by Molander and co-workers in 20% yield in refluxing THF.[49] This result was reproducible in our hands, but it generated a large quantity of brown oily solids that could be removed from **1** by washing with pentane. We were able to characterize one of the byproducts from the oil as monometallic $Cp^{An}YCl(THF)$.[50] Full characterization of $Cp^{An}YCl(THF)$, including the crystal structure, is provided in the Supporting Information. Ultimately, we found that the reaction of YCl_3 and K_2Cp^{An} in toluene at reflux afforded compound **1** in 39% yield. This route avoids THF entirely, does not generate the brown oil,

https://doi.org/10.1021/jacs.3c01405
J. Am. Chem. Soc. 2023, 145, 10730−10742

and affords **1** in the highest observed yield (see Table S1 for optimization).

Compound **1** reacts with $LiHBEt_3$ and $PhSiH_3$, but neither reaction forms the desired bridging hydride product. Instead, a hydrogenolysis route to the hydride was pursued. Both monometallic $Cp^{An}YCl(THF)$ and bimetallic **1** react with (allyl)MgCl in toluene to generate $Cp^{An}Y(C_3H_5)(THF)$, **2**, as a bright yellow solid, Scheme 1. THF is retained in the solid state, as shown in the X-ray crystal structure, Figure 1. In

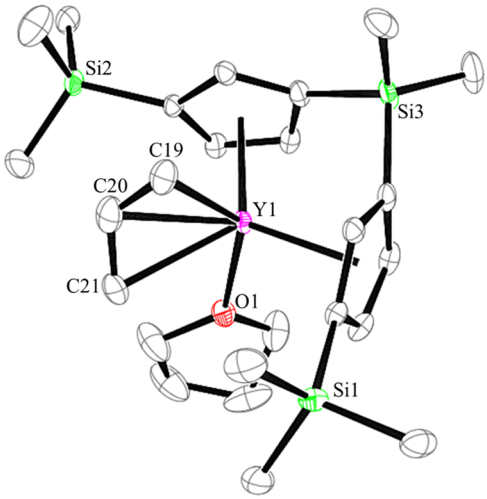

Figure 1. ORTEP diagram of $Cp^{An}Y(C_3H_5)(THF)$, **2**, with thermal ellipsoids drawn at the 50% probability level and selective atom labeling. Hydrogen atoms have been omitted for clarity.

comparison, both $(C_5Me_5)_2Y(\eta^3\text{-}C_3H_5)$ and $[Me_2Si(C_5Me_4)_2]Y(\eta^3\text{-}C_3H_5)$ were crystallographically characterized as the THF-free complexes, although each also forms a THF adduct.[51]

Treatment of bright yellow **2** with 80 psi of H_2 gas in the absence of solvent generated a colorless solid within 1 h. The product was crystallized from toluene to yield colorless single crystals of the yttrium hydride complex $[Cp^{An}Y(\mu\text{-}H)(THF)]_2$, **3**, identified by X-ray crystallography, Figure 2. Complex **3** has both cyclopentadienyl rings of each Cp^{An} ligand coordinated to just one metal center, which allows it to be compared with $[(C_5H_4Me)_2Y(\mu\text{-}H)(THF)]_2$,[52] $[\{(1,3\text{-}Me_2\text{-}C_5H_3)_2Y(THF)(\mu\text{-}H)\}_2]$,[53] and $\{[Me_2Si(C_5H_4)_2]Y(THF)(\mu\text{-}H)\}_2$,[54] Table 1. The metrical parameters for **3** are similar to those of other Y(III) hydrides. In particular, the Y···Y distance of 3.6311(5) Å in **3** falls within the typical values for other bimetallic bridging hydride complexes, including $\{[Me_2Si(C_5H_4)_2]Y(THF)(\mu\text{-}H)\}_2$ [3.514(3) Å],[54] $\{[Y(Me_3TACD)(THF)(\mu\text{-}H)]_2\}[B(3,5\text{-}C_6H_3[CF_3]_2)_4]_2$ [3.6203(9) Å, TACD = 1,4,7,10-tetramethyl-1,4,7,10-tetraazacyclododecane],[55] $[\{(MeC_5H_4)_2Y(THF)(\mu\text{-}H)\}_2]$ [3.66(1) Å],[52] $[\{(dadmb)Y(THF)(\mu\text{-}H)\}_2]$ [3.6652(8) Å, dadmb = 2,2′-bis-[(*tert*-butyldimethylsilyl)amido]-6,6′-dimethylbiphenyl],[56] $[\{SiMe_2(C_5Me_4)(N^tBu)Y(THF)(\mu\text{-}H)\}_2]$ [3.672(1) Å],[57] $[\{(1,3\text{-}Me_2\text{-}C_5H_3)_2Y(THF)(\mu\text{-}H)\}_2]$ [3.68(1) Å],[53] and $\{Y[(Me_3Si)_2NC(N^iPr)_2]_2(\mu\text{-}H)\}_2$ [3.6825(5) Å].[58]

Crystallization of $[(\mu\text{-}Cp^{An})Y(\mu\text{-}H)]_2$, 3′. During an attempted reduction of **3** (vide infra), crystals of another Cp^{An} yttrium hydride, $[(\mu\text{-}Cp^{An})Y(\mu\text{-}H)]_2$, **3′**, Figure 3, were obtained co-crystallized with $[K(crypt)][Cp^{An}Y(C_3H_5)(H)]$. Presumably, some remnant of **2** was carried over to the

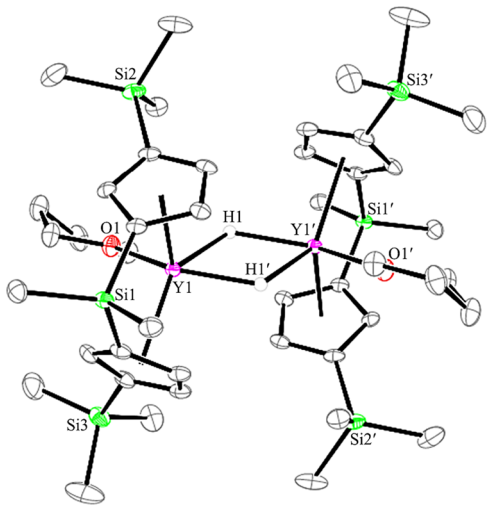

Figure 2. ORTEP diagram of $[Cp^{An}Y(\mu\text{-}H)(THF)]_2$, **3**, with thermal ellipsoids drawn at the 50% probability level and selective atom labeling. Hydrogen atoms, except the hydride ligands, have been omitted for clarity.

reaction of **3** with KC_8 and crypt. While the X-ray structure revealed a "flyover" structure for this hydride in which the Cp^{An} ligands are coordinated to two different metals, the diffraction data were too poor to discuss metrical parameters. The isolation of this species, which differs from **3** in that there is no solvated THF, suggests that small changes can affect the "flyover" versus non-bridging coordination of the Cp^{An} ligand.

Reduction of $[Cp^{An}Y(\mu\text{-}H)(THF)]_2$, 3. The reaction of colorless **3** with excess KC_8 and one equivalent of crypt in THF at −30 °C produced an intensely colored red-brown solution. After crystallization, dark red-brown crystals of $[K(crypt)][(\mu\text{-}Cp^{An})Y(\mu\text{-}H)]_2$, **4**, were isolated, Scheme 1, Figure 4, which is formally an Y(III)/Y(II) complex.

The asymmetric unit of **4**, Figure 4, consists of one $[K(crypt)]^{1+}$ and two half-molecules of the bimetallic anion $\{[(\mu\text{-}Cp^{An})Y(\mu\text{-}H)]_2\}^{1-}$. A crystallographic inversion center is present at the center of the $Y_2(\mu\text{-}H)_2$ core, thus yielding two independent $\{[(\mu\text{-}Cp^{An})Y(\mu\text{-}H)]_2\}^{1-}$ anions in the unit cell. The metrical parameters involving the metal centers of the two crystallographically distinct bimetallic anions are equivalent within three standard deviations.

The binding mode of the Cp^{An} ligand in **4** differs from those in **1**−**3** in that it has a bridging "flyover" structure with coordination to both metals. This has been previously observed for $[(\mu\text{-}Cp^{An})Sm(\mu\text{-}H)(THF)]_2$[46] and $[(\mu\text{-}Cp^{An})Y(\mu\text{-}H)]_2$, **3′**, described above. The 3.3992(6) and 3.4022(7) Y···Y distances in **4** are significantly shorter than the 3.635(4) and 3.596(2) Å distances reported for a fullerene complex that is described as having Y−Y bonds.[34] The Y···Y distances in **4** are also more than 0.3 Å shorter than the 3.727(1) Å distance in $[(C_5{}^iPr_5)Y]_2(\mu\text{-}I)_3$, which is analyzed as a metal−metal bonded complex.[47] The Y···Y distances in **4** are the shortest Y···Y distances in the literature, to our knowledge, Table 2.

Spectroscopy of 4. Solution-phase X-band EPR spectra of **4** in THF were obtained at 77 K and room temperature, Figure 5. The room temperature EPR spectrum contains a two-line pattern at g_{iso} = 1.99 with a hyperfine coupling constant of A = 40 G. The spectra are similar to the EPR spectra of crystallographically characterized $[K(crypt)][Cp'_3Y]$ (g_{iso} = 1.991, 36.6 G)[23] and the product of KC_8 reduction of Cp''_3Y

https://doi.org/10.1021/jacs.3c01405
J. Am. Chem. Soc. 2023, 145, 10730−10742

Table 1. Comparison of Selected Bond Distances (Å) and Angles (°) for $[Cp^{An}Y(\mu\text{-}H)(THF)]_2$, **3**, $[(C_5H_4Me)_2Y(\mu\text{-}H)(THF)]_2$,[52] $[\{(1,3\text{-}Me_2\text{-}C_5H_3)_2Y(THF)(\mu\text{-}H)\}_2]$,[53] and $\{[Me_2Si(C_5H_4)_2]Y(THF)(\mu\text{-}H)\}_2$[54]

	$[Cp^{An}Y(\mu\text{-}H)(THF)]_2$, **3**	$[(C_5H_4Me)_2Y\text{-}(\mu\text{-}H)(THF)]_2$[52]	$[\{(1,3\text{-}Me_2C_5H_3)_2\text{-}Y(THF)(\mu\text{-}H)\}_2]$[53]	$\{[Me_2Si(C_5H_4)_2]Y\text{-}(THF)(\mu\text{-}H)\}_2$[54]
Y···Y′	3.6311(5)	3.664(1)	3.68(1)	3.514(3)
Y−Cnt	2.457	2.4114	2.434	2.357
	2.392	2.397	2.391	2.315
Y−H	2.25(3)	2.19(8)	2.27(6)	2.44(7)
	2.03(3)	2.17(8)	2.03(7)	2.04(7)
Y−H−Y′	116(1)	114(3)	117.7(27)	103(3)
H−Y−H′	63.9(13)	66(3)	62.3(27)	77(3)

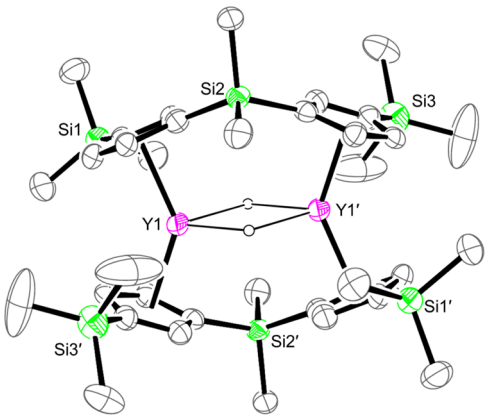

Figure 3. Connectivity plot of $[(\mu\text{-}Cp^{An})Y(\mu\text{-}H)]_2$, **3′**, with selective atom labeling. Co-crystallized $[K(crypt)][Cp^{An}Y(C_3H_5)(H)]$, THF, and hydrogen atoms, except for the bridging hydrides, have been omitted for clarity.

(g_{iso} = 1.9908, 36.1 G),[59] except that the *A* value is slightly higher. Reduction of $[Cp'_2Y(\mu\text{-}Me)]_2$ gave an EPR signal at g_{iso} = 1.99 with *A* = 18.4 G, but that reduction product was not structurally characterized.[42] Potassium graphite reductions of other monometallic cyclopentadienyl yttrium complexes gave higher *A* values: $(C_5H_5)_3Y(THF)$ (g_{iso} = 1.9905, *A* = 42.8 G)[59] and $(C_5H_4Me)_3Y(THF)$ (g_{iso} = 1.9903, *A* = 46.9 G).[59] Crystallographically characterized $[K(18\text{-crown-}6)_2]\{Y[N(SiMe_3)_2]_3\}$ (g_{iso} = 1.976, *A* = 110 G)[60] and $[K(crypt)][Y(OC_6H_2Ad_2\text{-}2,6\text{-}^tBu\text{-}4)_3]$ (g_{iso} = 1.98, *A* = 153.3 G)[61] had analogous EPR spectra with even higher *A* values. The hyperfine coupling constant *A* in these Y(II) complexes seems to correlate with the electron donation strength[27] of the ligand,[59,62,63] and the *A* value for **4** is in line with the expected trend.

The solid-state EPR spectrum of **4** displayed a rhombic signal with *g* values of 2.00, 1.99, and 1.97, with no apparent coupling to an yttrium or hydrogen nucleus, Figure S4. This is consistent with the theoretical analysis below that shows little unpaired spin density on the hydrogen atoms. For comparison, the EPR spectrum of $[(C_5{}^iPr_5)Y]_2(\mu\text{-}I)_3$ at 10 K shows an axial signal with no discernible yttrium splitting.[47]

The UV−visible spectrum of the dark red-brown compound **4** in THF displays a broad absorption band at 410 nm with an attenuation coefficient of approximately 1680 M^{-1} cm^{-1} that is not present in the spectrum of colorless **3**, Figure S5. This spectrum is similar to the spectra observed for the Y(II) complexes $[K(crown)][Cp'_3Y]$ and $[K(crypt)][Cp'_3Y]$, which have absorption bands at 530 nm (ε = 2500 M^{-1} cm^{-1})[23] and 520 nm (ε = 4500 M^{-1} cm^{-1}),[21,28] respectively. In comparison, the spectrum of the reduction product of $[Cp'_2Y(\mu\text{-}H)(THF)]_2$[42] has an absorption band at 794 nm (ε = 1000 M^{-1} cm^{-1}), which is red-shifted compared to **4**. The near-IR (NIR) spectrum of **4** in THF showed no absorptions that could be attributed to an intervalence charge transfer (IVCT) band. The absorption bands of **4** do not shift in Et_2O.

Magnetic Susceptibility of $[K(18\text{-crown-}6)(THF)_2][(\mu\text{-}Cp^{An})Dy(\mu\text{-}H)]_2$, 5. A dysprosium analogue of the anion in **4** was synthesized by an analogous route to Scheme 1 using 18-crown-6 instead of crypt, Scheme 2. The complex $[K(crown)(THF)_2][(\mu\text{-}Cp^{An})Dy(\mu\text{-}H)]_2$, **5**, was characterized by X-ray crystallography, but the data were not of high enough quality to discuss metrical parameters, see Figure S10. Reductions in

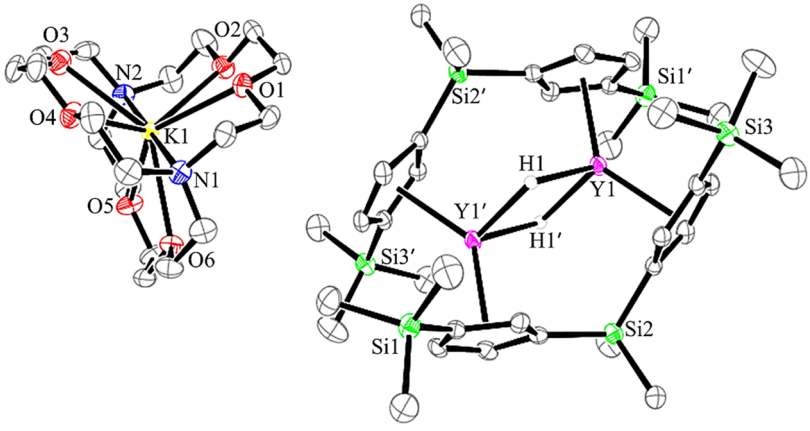

Figure 4. ORTEP diagram of $[K(crypt)][(\mu\text{-}Cp^{An})Y(\mu\text{-}H)]_2$, **4**, showing one of the two crystallographically independent $\{[(\mu\text{-}Cp^{An})Y(\mu\text{-}H)]_2\}^{1-}$ anions in the unit cell with thermal ellipsoids drawn at the 50% probability level. Hydrogen atoms, except the hydride ligands, have been omitted for clarity.

https://doi.org/10.1021/jacs.3c01405
J. Am. Chem. Soc. 2023, 145, 10730−10742

Table 2. Comparison of Distances (Å) and Angles (°) between 3, 4, $[(C_5{}^iPr_5)Y]_2(\mu\text{-}I)_3$, and $\{[(C_5H_4)_2SiMe_2]Y(\mu\text{-}H)(THF)\}_2$[a]

	3	4	$\{[(C_5H_4)_2SiMe_2]Y(\mu\text{-}H)(THF)\}_2$	$[(C_5{}^iPr_5)Y]_2(\mu\text{-}I)_3$
Y−Cnt1	2.392	2.358, 2.362	2.315	2.337
Y−Cnt2	2.457	2.358, 2.367	2.357	
Cnt1−Y−Cnt2	119.9	135.4, 137.5	129.5	
Y···Y	3.6311(5)	3.3992(6), 3.4022(7)	3.514(3)	3.727(1)

[a]Compound 4 has two independent molecules in the unit cell.

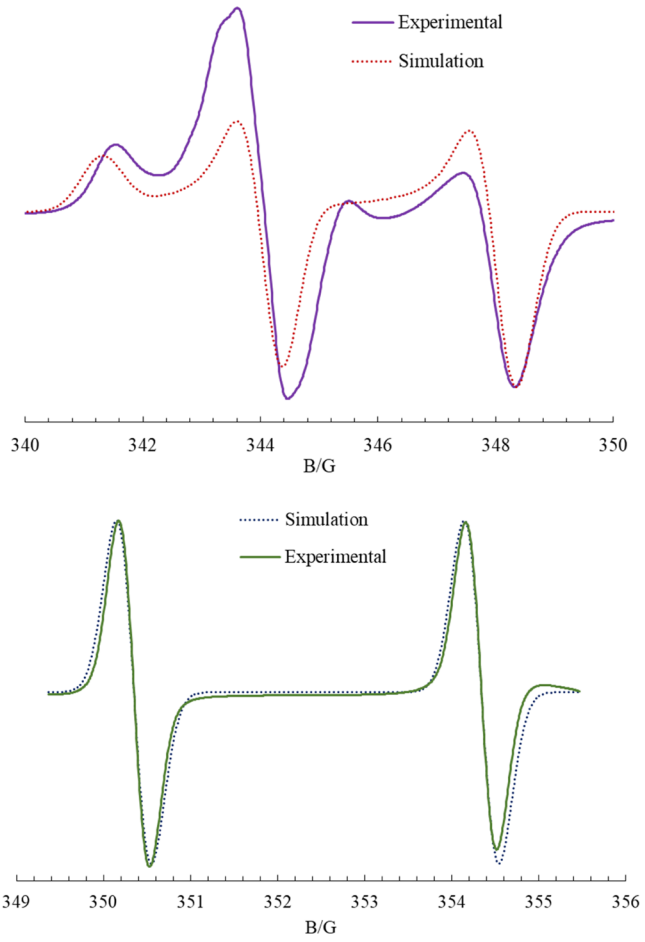

Figure 5. Solution-phase EPR spectra of 4 at 77 K (top, purple (experimental), dotted red (simulation); g_1 = 1.99, A_1 = 35 G; g_2 = 2.00, A_2 = 21 G) and room temperature (bottom, green (experimental), dotted blue (simulation); g_{iso} = 1.99, A = 40 G) in THF.

the presence of crypt instead of 18-crown-6 led to the formation of amorphous dark brown crystals, likely the $[K(crypt)]^{1+}$ analogue of 5, but we could not confirm the structure. The Cp^{An} binding modes between the Y and Dy compounds are identical, i.e., compound 5 has a "flyover" structure like that observed for 3′ and 4, while the Dy(III) precursor $[Cp^{An}Dy(\mu\text{-}H)(THF)]_2$ had both rings of the Cp^{An} ligand bound to a single metal like what was observed for 3, Scheme 2.

The variable temperature magnetic susceptibility of 5 was examined to determine if it exhibited magnetic coupling interactions between the two Dy centers. Complex 5 exhibited a room temperature $\chi_M T$ value of 30.04 emu K mol^{-1} under an applied dc magnetic field of 0.1 T, which is only slightly lower than the predicted value of 31.18 emu K mol^{-1} for a dinuclear complex containing one Dy^{3+} ion ($4f^9$) and one Dy^{2+} ion with an $L-S$ coupled $4f^9(5d_{z^2})^1$ electron configuration, Figure 6.

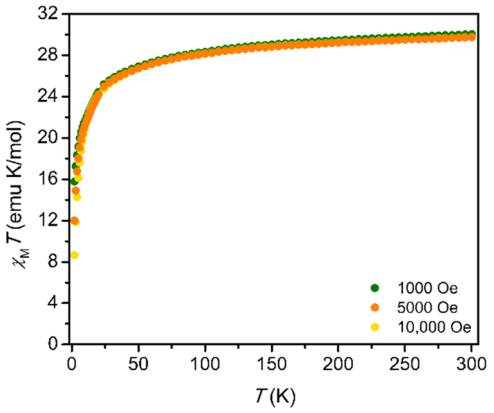

Figure 6. $\chi_M T$ plot for 5.

The predicted room temperature $\chi_M T$ value for an $L-S$ coupled Dy^{2+} ion was calculated using L = 5 and $S = S_{5dz2} + S_{4f}$ = 3.[48] In contrast, the value for $[(C_5{}^iPr_5)Dy]_2(\mu\text{-}I)_3$ was 51.77 emu K mol^{-1},[47] which is consistent with the parallel alignment of the electrons on both Dy centers as a result of a single-electron Dy−Dy bond. At low temperatures, a decline in the $\chi_M T$ product of 5 is observed due to thermal depopulation of the M_J manifolds of the Dy ions. Quantitative analysis of the magnetic exchange coupling in 5 is challenging due to the anisotropic nature of Dy^{3+} and Dy^{2+}; however, dc magnetic susceptibility data suggest that the two Dy ions in 5 do not

Scheme 2. Synthesis of $[K(crown)(THF)_2][(\mu\text{-}Cp^{An})Dy(\mu\text{-}H)]_2$, 5

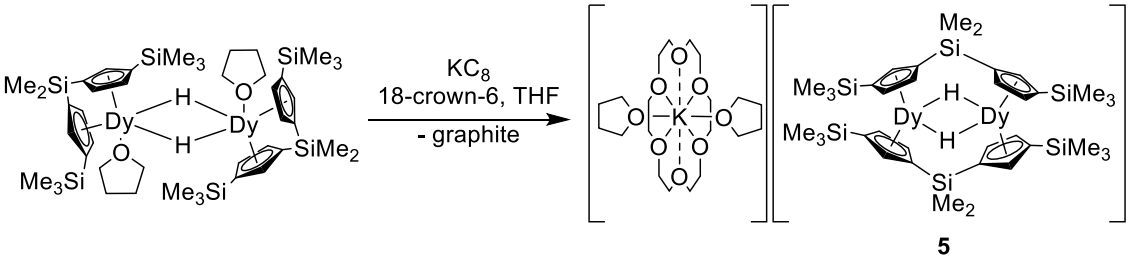

https://doi.org/10.1021/jacs.3c01405
J. Am. Chem. Soc. 2023, 145, 10730−10742

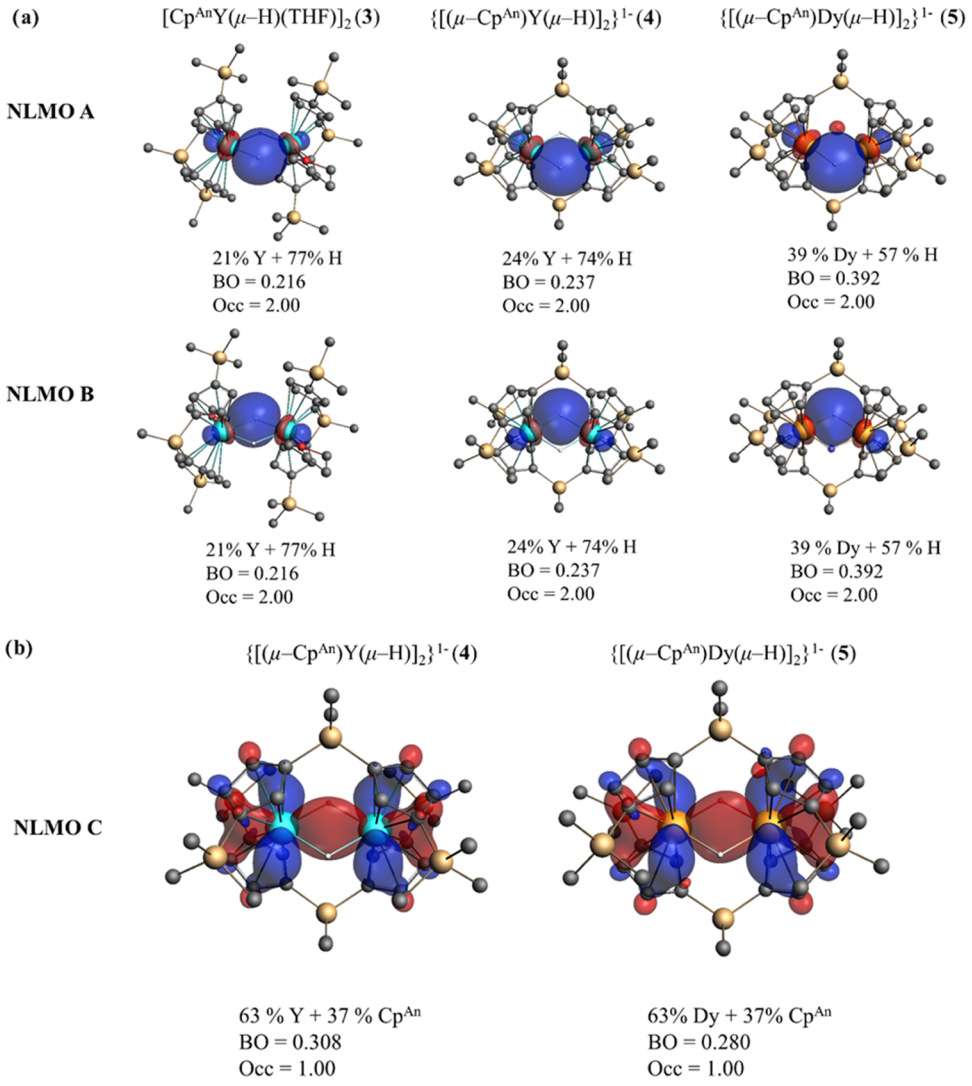

Figure 7. Selected natural localized molecular orbitals (NLMOs) depicting the interaction between Y centers (cyan) in $[Cp^{An}Y(\mu\text{-H})(THF)]_2$, **3**, $\{[(\mu\text{-}Cp^{An})Y(\mu\text{-H})]_2\}^{1-}$, **4**, and $\{[(\mu\text{-}Cp^{An})Dy(\mu\text{-H})]_2\}^{1-}$, **5**. The localized bond order (BO) contribution, NLMO hybrid composition, and occupation numbers (Occ) are also shown. (a) NLMO A and NLMO B show the electron-deficient 3-center 2-electron bonds involving the metal–hydride–metal interaction for the three complexes; (b) NLMO C shows the 2-center 1-electron Y–Y bond. The total metal–metal localized BOs are 0.080 (Y^{III}–Y^{III}), 0.540 (Y^{II}–Y^{III}), and 0.649 (Dy^{II}–Dy^{III}) for **3**, **4**, and **5**, respectively.

interact strongly with each other. In sum, the dc magnetic susceptibility data suggest that there is not a single-electron Dy–Dy bond in **5**. No out-of-phase signals were observed in the ac susceptibility measurements, indicating that **5** is not a single-molecule magnet. Magnetic hysteresis measurements collected at 2 K show a slight opening at applied fields, likely the result of intermolecular interactions, Figure S2.

Theoretical Analysis of $[Cp^{An}Y(\mu\text{-H})(THF)]_2$, 3, and $\{[(\mu\text{-}Cp^{An})Y(\mu\text{-H})]_2\}^{1-}$, 4. Bonding. To better understand the electronic structures of **3** and **4**, the natural localized molecular orbital (NLMO) formalism was considered (see Computational Details). The advantage of transforming canonical molecular orbitals (MOs) into NLMOs is that the resulting picture of the chemical bond is closer to that of chemical intuition but still delocalized enough to resemble canonical MOs.[64] The results show two main interactions for complex **3** and three for complex **4**, Figure 7. As previously predicted for this type of hydride-bridged complexes,[42] electron-deficient 3-center 2-electron bonds are displayed in NLMO A and NLMO B, Figure 7a, which are common to both structures. NLMO A and NLMO B are equivalent in composition, where the two hydrogen 1s electrons form delocalized bonding orbitals with the empty Y 4d shell. While the NLMO compositions for **3** are 77% H [1s] + 21% Y [0.16 5s + 0.84 4d], in **4**, the polarization of the bond is calculated to be slightly less at 74% H [1s] + 24% Y [0.20 5s + 0.80 4d]. This difference does not have a significant impact on the associated bond orders (BOs), as the difference in BO between **3** and **4** is only 0.021.

An additional interaction is observed in the reduced species **4**, where the added electron forms a σ-bond between the two Y centers involving their 4d orbitals (NLMO C). The two metal centers equally contribute 63% of the total NLMO, while the remaining 37% is delocalized on the Cp^{An} rings, Figure 7b. Although a formal Y···Y interaction is represented by NLMO C, it is only half occupied and highly delocalized on the Cp^{An} ligands, with a natural localized BO of only 0.308. Furthermore, each Y center has 0.314 and 0.323 unpaired electrons predicted by NBO, while both bridging hydrogen atoms show nearly null spin density with a value of −0.01.

https://doi.org/10.1021/jacs.3c01405
J. Am. Chem. Soc. 2023, 145, 10730−10742

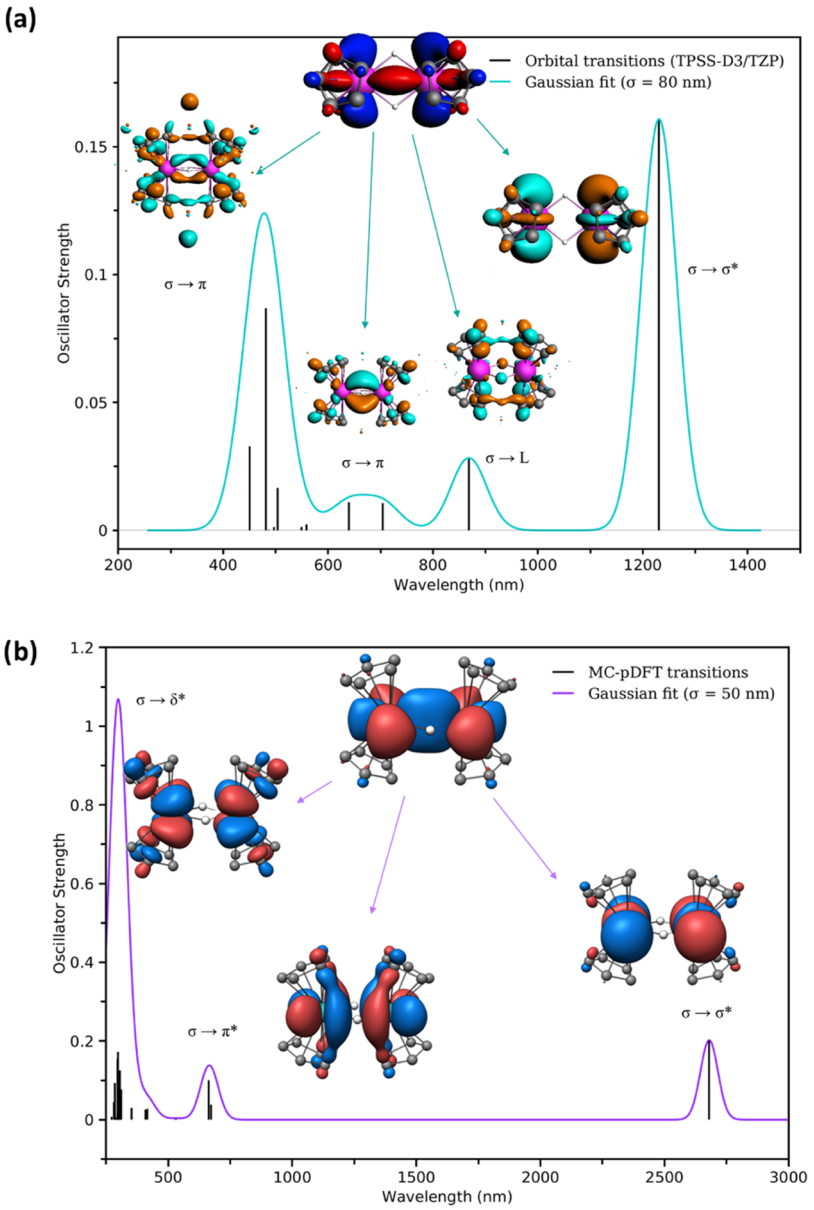

Figure 8. Calculated absorption spectra of **4** using (a) TD-DFT (TPSS-D3/STO-TZP) and (b) MC-pDFT (ANO-RCC-TZP). Depiction of selected orbitals involved in vertical transitions were included as insets for each panel, with silyl substituents of the Cp^{An} removed for clarity. The MC-pDFT structure was simplified to make the calculation feasible. Given the multiconfigurational character of the MC-pDFT states involved in the predicted spectrum, the $\sigma \rightarrow \delta^*$ band seems more intense than the other band, but this is only because of the overlapping states in a small range of wavelengths. The most intense individual transition is the $\sigma \rightarrow \sigma^*$ with an oscillator strength of 0.16 and 0.20 for TD-DFT and MC-pDFT methods, respectively.

Spectroscopy. Given the unique electronic structure of the ground state (GS) found through the localization analysis for complex **4**, we explored the interaction between the GS and excited states (ES). To do so, time-dependent DFT (TD-DFT) and multiconfigurational pair-density functional theory (MC-pDFT) calculations were combined to predict the vertical transitions and their oscillator strengths involved in the absorption spectrum, particularly focusing on the lower energy transitions. Both methods suggest that vertical GS → ES transitions occur from the singly occupied σ-bonding orbital to σ^*, π^*, δ, and δ^* orbitals, Figure 8. The lowest energy transition that corresponds to the $\sigma \rightarrow \sigma^*$ transition had the highest oscillator strength, with values of 0.16 and 0.20 for TD-DFT and MC-pDFT, respectively. The difference in the two calculated spectra emphasizes the complexity of the system and how difficult it is to reproduce the IVCT band in mixed valent systems.[65] It is noteworthy that these results are based on vertical excitations using the molecular orbitals corresponding to the ground state. Therefore, these results provide information solely of the nature of the ground state and not low-lying states, as discussed below in the Magnetism section.

Theoretical Analysis of $\{[(\mu\text{-}Cp^{An})Dy(\mu\text{-}H)]_2\}^{1-}$, 5. Bonding. The Dy compound **5** had a similar bonding situation as **4**, Figure 7. The 3-center 2-electron bonding orbitals (NLMOs A and B) have 39% Dy contribution, with 6s and 5d compositions ranging from 27−43 and 55−72%, respectively. NLMO C suggests a Dy···Dy interaction and has a 63% contribution from the Dy atoms, which are composed of mostly 5d orbital contribution (96%) and a small amount of 6s

https://doi.org/10.1021/jacs.3c01405
J. Am. Chem. Soc. 2023, 145, 10730−10742

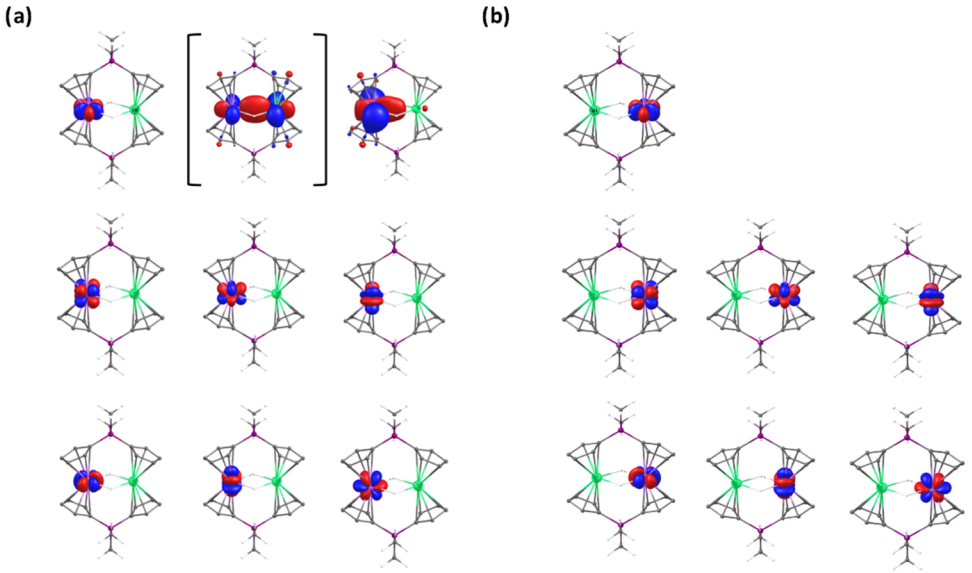

Figure 9. State average molecular orbitals for the (a) Dy^{II}–Lu^{III} and (b) Dy^{III}–Lu^{III} models at spin-free CASSCF level. The molecular orbital shown in brackets (metal–metal σ-bond) results from a state-specific calculation of the ground state instead of the partially localized $5d_{z^2}$ orbital obtained from the state average calculation.

Table 3. Relative Energies (cm^{-1}) and *g*-Factors of the Crystal Field States of the Ground Multiplet $^6H_{15/2}$ of the Dy^{III} Ion in Dy^{III}–Lu^{III} Complex from SO-CASSCF/Single_Aniso Calculations

energy (cm^{-1})	g_x	g_y	g_z	wavefunction composition
0.0	0.007	0.017	19.493	79%|±15/2> + 14%|∓15/2>
132.3	0.209	0.344	16.478	74%|±13/2> + 14%|∓13/2>
212.3	2.281	2.857	16.303	20%|±1/2> + 18%|∓3/2> + 16%|∓7/2> + 14%|±1/2> + 14%|∓11/2>
247.3	0.856	4.543	10.053	62%|±11/2>
295.2	8.215	6.723	4.482	31%|±9/2> + 20%|∓9/2> + 12%|±5/2>
327.6	1.658	2.486	13.652	36%|∓7/2> + 17%|±1/2> + 15%|±9/2> + 10%|±5/2>
398.0	0.060	0.082	17.263	30%|∓5/2> + 24%|±7/2> + 18%|±3/2>
605.7	0.000	0.001	19.862	38%|±1/2> + 30%|∓3/2> + 17%|±5/2>

character (4%). Interestingly, unlike **4**, NLMO C has an unequal 56:44 contribution ratio from the two Dy centers. This may be a reason that the BO of the corresponding NLMO C in **5** is slightly lower than in **4** (0.280 vs 0.308). The spin densities of the Dy centers are 5.30 and 5.23 unpaired electrons, which further suggests that the added electron resides (unequally) on both Dy centers. The bridging hydrogen atoms display negligible values of −0.01 unpaired electrons.

It is worth mentioning the uniqueness of these systems from an electronic structure perspective. Usually, electronic properties of f-element complexes can be reproduced by calculation irrespective of whether the orbital set used is state-specific or an average of low-lying states. This is common with f-electron configurations due to the closely spaced f-orbital manifold. However, given that the electron of interest in **4** and **5** is not located in an f orbital, the optimized orbital set may vary even within the low-lying states. This causes the bonding situation to differ in excited states with respect to the ground state, where the metal–metal bonding weakens significantly due to partial localization of the electron on one of the two metal centers, Figure 9.

Magnetism. The complete active space self-consistent field (CASSCF) approximation was used to perform magnetic analyses on **5** by substituting one Dy atom with a diamagnetic Lu atom (see Computational Details). This approach allows the magnetic properties of a pair of f ions to be evaluated and compared to a magnetically isolated analogue and is mainly used when the dimensions of the configuration space in a system are beyond the practical scope of the methodology used to the exploration of the entire magnetic exchange spectrum. Given that the ground-state calculations above, Figure 7, showed that the SOMO orbital is a σ-bonding orbital between both metal ions, the substitution was done to best retain this interaction. Despite the changes introduced in the symmetry of the σ-orbital and metal contributions, the properties found in this Dy–Lu approximation are in good agreement with those determined in the experiment. Two scenarios were considered, Dy^{III}–Lu^{III} and Dy^{II}–Lu^{III}, and from these combinations, the χT vs T behavior was studied. The molecular orbitals for both models are shown in Figure 9.

Dy^{III}–Lu^{III}. The local properties can be described from the ground multiplet $^6H_{15/2}$, which, due to crystal field effects, splits into eight Kramers doublets, Table 3. The analysis of the *g*-factors of these states reveals a strong magnetic anisotropy of the ground doublet dominated by the larger values of m_J, which rapidly deteriorates for the rest of the members of the manifold. Thus, only the ground Kramers doublet has an easy axis, and a magnetization barrier is not expected for one isolated Dy^{III} center.

Dy^{II}–Lu^{III}. As a second step in the study, the Dy^{II}–Lu^{III} system was analyzed with one electron in the sigma orbital,

https://doi.org/10.1021/jacs.3c01405
J. Am. Chem. Soc. 2023, 145, 10730–10742

using a CAS(10,8)SCF active space, including 28 roots for both the $S = 3$ and $S = 2$ states. The $S = 2$ state was explicitly considered to investigate the role of the SOMO electron through analyzing contributions to the wavefunction of spin-flip states. The analysis of the CASSCF wave functions revealed the high spin configuration ($S = 3$, septet) makes up the ground state, while the first quintet state possesses a spin-flip configuration of the σ-electron. This allows the Dy center to retain its high spin configuration as in the trivalent ion (ferromagnetic coupling between the 4f and σ-bonding electrons). The energy difference between the septet and quintet states is ~1640 cm^{-1}, indicating a strong Dy−σ spin−spin coupling. This was also (qualitatively) corroborated by DFT calculations through the broken-symmetry formalism (Table 5). Table 4 summarizes the energies and contributions

Table 4. Relative Energies (cm^{-1}) of the Low-Lying Spin−Orbit States Obtained from the Interaction of ^7H and ^5H Terms in Dy^{II}−Lu^{III} Complex (SO-CASSCF Calculations)

energy (cm^{-1})	wavefunction composition
0.0	94%|$^7H_8$>
328.9	92%|$^7H_8$>
496.9	93%|$^7H_8$>
573.7	85%|$^7H_8$>
748.7	86%|$^7H_8$>
2476	32%|^5H > + 29%|^7H>[a]

[a]First state with a large contribution of the \|^5H> term.

of the low-lying spin−orbit coupling states to the $^7H_8$ term obtained from the interaction between all septets and quintets in an SO-CASSCF calculation (see Computational Details).

Based on the above results, an appropriate model to describe the behavior of χT vs T would be to evaluate the interaction between two centers locally understood as a Dy^{III} metal center and a single electron in the σ bonding orbital. The calculated room temperature χT value for the Dy^{III} center in the Dy^{III}−Lu^{III} complex was 13.96 emu K mol^{-1}, which is slightly lower than the 14.15 emu K mol^{-1} value predicted for a free Dy^{III} ion. Similarly, the calculated room temperature χT product for the Dy^{III}−σ (^7H) electron was 16.50 emu K mol^{-1}. Thus, at room temperature, the total χT value is 30.47 emu K mol^{-1}. This deviates slightly from the experimental value of 30.04 emu K mol^{-1} but coincides with the sum of the individual susceptibilities of each metal center, indicating that there is no relevant interaction between the two Dy centers.

The χT profile shown in Figure 10 was calculated with an exchange coupling parameter of $J = 0$ cm^{-1} between both magnetic centers. The plot shows a similar result to that obtained from the simple sum of the profiles of both individual centers, which suggests that there is a balance between the Dy^{III}−σ exchange interaction and the dipolar interaction between the metal centers resulting in a null or negligible interaction in the structure. In the temperature range analyzed (0.1−300 K), a decrease in the χT product was observed as the temperature decreased, consistent with a nonferromagnetic interaction between both metal centers. It is possible to rule out an antiferromagnetic interaction considering that the χT value at low temperature is far from the expected $S = 1/2$ value of 0.37 emu K mol^{-1}. The analysis of the molecular χT behavior allows us to conclude that in the temperature range measured, the values are equivalent to the sum of the individual center behavior, and no evidence of direct Dy−Dy

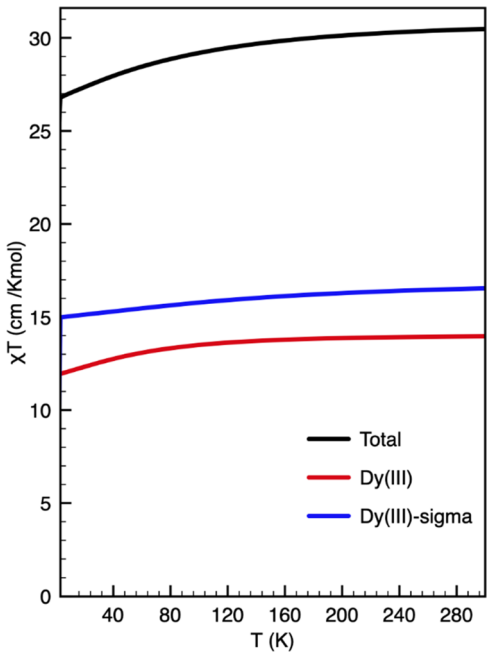

Figure 10. χT vs T profile for the local centers and the whole molecule of **5** obtained considering a coupling parameter $J = 0$ cm^{-1}.

magnetic interaction was found, consistent with the observed magnetic data in Figure 6. Additional calculations with $J = -0.1$, -0.5, or -1.0, Figure S1, provided a significantly worse fit to the experimental data. The temperature dependence of χT can be unequivocally attributed to the progressive depopulation of excited states upon decreasing the temperature (Table 5).

Table 5. Magnetic Coupling Constants, J and J' (cm^{-1}), Describing the Dy−σ-Electron and Dy−Dy Coupling, Respectively[a]

DFT functional	J (Dy−σ-electron)	J' (Dy−Dy)
B3LYP (40% HF exchange)	194	−35
B3LYP (30% HF exchange)	143	+16
PBE0 (25% HF exchange)	68	+2
B3LYP (20% HF exchange)	80	+6

[a]J values were calculated under the broken-symmetry formalism with two different functionals varying the HF exchange contribution.

DISCUSSION

In contrast to reductions of $[Cp'_2Y(\mu\text{-H})]_2$, $[Cp'_2Y(\mu\text{-Me})]_2$, and $[Cp'_2Y(\mu\text{-Cl})]_2$, which give intensely colored products with EPR spectra consistent with the presence of Y(II), but no isolable crystalline material, reduction of the *ansa*-cyclopentadienyl hydride $[Cp^{An}Y(\mu\text{-H})(THF)]_2$, **3**, gives the crystalline complex $[K(crypt)][(\mu\text{-}Cp^{An})Y(\mu\text{-H})]_2$, **4**. The chelating nature of the Cp^{An} ligand likely disfavors ligand rearrangement,[62] which occurred with the Cp′ reductions and allows stabilization and crystallization of the reduced complex. The intense color and EPR spectra of **4** are consistent with the presence of Y(II), and the crystallographic data show that both yttrium ions are equivalent by symmetry. Since there are no low-lying acceptor orbitals, complex **4** does not bind THF,[66] and the change in the binding mode of the Cp^{An} ligand between **3** and **4** is likely a result of minimizing steric

https://doi.org/10.1021/jacs.3c01405
J. Am. Chem. Soc. 2023, 145, 10730−10742

interactions. This is consistent with the "flyover" structure of **3′**, the unsolvated analogue of **3**.

The X-ray crystal structure of **4** reveals the shortest Y···Y distances observed to date, 3.3992(6) and 3.4022(7) Å. These distances are 0.2−0.3 Å shorter than those in complexes described as exhibiting Y−Y bonding interactions with a bond order of 0.5, including the 3.635(4) and 3.596(2) Å distances in a fullerene complex[34] and the 3.727(1) Å distance in $[(C_5{}^iPr_5)Y]_2(\mu\text{-}I)_3$.[47] Although short metal−metal distances are suggestive of metal−metal bonding, it is well known that these distances can be deceiving.[67−70]

DFT studies suggest a ground state containing a delocalized metal−metal half-bond via the 4d orbitals of the yttrium metal centers in **4** consistent with the short Y···Y distance. However, the EPR spectrum suggests localized behavior for the unpaired electron, whereas the UV−visible spectrum results are difficult to interpret due to the lack of obvious IVCT absorption bands. This type of spectroscopic and crystallographic disparity is common with Robin−Day[71] Class II−III complexes.[72−74] The solvent-independent nature of the absorptions is also found with Class II−III compounds.[52] The sigma bonding orbital is only found in the state-specific molecular orbitals of the ground state, which suggests the metal−metal bonding interaction is unique to the ground state and not to the low-lying states, which ultimately affects the magnetic susceptibility of the molecule.

It is interesting how the Cp^{An} metallocene and bridging hydride environments complicate the analysis compared to the mono-cyclopentadienyl complexes $[(C_5{}^iPr_5)Ln]_2(\mu\text{-}I)_3$,[47] which are assigned as Robin−Day Class III compounds. For example, $[(C_5{}^iPr_5)Y]_2(\mu\text{-}I)_3$ exhibits $\Gamma \approx 0.6$, which is characteristic of Class III delocalization.[73,74] This may be a result of the Cp^{An} ligand orbitals mixing into the sigma bonding orbital of **4** and **5**, Figure 7, whereas the $[(C_5{}^iPr_5)Ln]_2(\mu\text{-}I)_3$ examples have purely metal-based orbitals. The differences may also arise due to the presence of two electron-deficient hydride bridges in **4** and **5** versus three electron-precise iodide bridging groups in $[(C_5{}^iPr_5)Ln]_2(\mu\text{-}I)_3$, which may channel an added electron into a metal−metal bond.

Magnetic and theoretical analyses of the dysprosium analogue, $[K(18\text{-crown-}6)(THF)_2][(\mu\text{-}Cp^{An})Dy(\mu\text{-}H)]_2$, **5**, suggest that the metals have no interaction via the 4f orbitals as in the yttrium complex. DFT studies indicate that although there is an NLMO in **5** involving 5d orbitals similar to that for **4** with 4d orbitals, the contributions from each metal are not equal. Magnetic analysis indicates separate Dy^{III} and Dy^{III}-(5d) units, where the apparent noninteracting Dy centers can be explained by the thermal population of low-lying excited states that have negligible metal−metal interactions. Thus, while the Cp^{An} ligand is a good platform for bringing two metals in close proximity, the bridging hydride atoms may not be ideal for facilitating bimetallic magnetic interactions.

We hypothesize that the lack of out-of-phase ac signals for the Dy complex arises from transverse anisotropy induced by the hydride ligands. Hydride ligands have been previously proposed[75] to induce a strong crystal field splitting for Dy^{3+}, and for compound **5**, this would counteract the axial crystal field splitting of the cyclopentadienyl ligands to produce a more isotropic environment for the Dy^{3+} ion. Such transverse anisotropy would be expected to result in a lower value of U_{eff} and faster relaxation. In addition, the Dy^{2+} ion in compound **5** is a non-Kramer's ion in the divalent state, which would also promote fast magnetic relaxation. The presence of a nearby, quickly relaxing ion could also result in fast relaxation for the Dy^{3+} site (this situation represents the opposite of the classic magnetic dilution experiment, which promotes slow relaxation). Combined, these factors likely explain why we do not observe out-of-phase signals in the ac susceptibility.

CONCLUSIONS

The reduction of $[Cp^{An}Y(\mu\text{-}H)(THF)]_2$, **3**, with excess KC_8 and one equivalent of 2.2.2-cryptand produced the mixed-valence complex $[K(crypt)][(\mu\text{-}Cp^{An})Y(\mu\text{-}H)]_2$, **4**, whose X-ray crystal structure contains the shortest Y···Y distance observed to date in a molecular complex. Theoretical calculations of the ground state indicate that the SOMO involves a metal−metal bonding interaction between 4d orbitals on both metal centers with significant contributions from ligand orbitals. This delocalized view, which is consistent with the symmetric crystal structure, does not, however, match the EPR and UV−visible data, which suggest valence localization. Interestingly, the partial localization is recovered when state average orbitals are considered, where the metal−metal bonding orbital localizes toward one of the two metal centers as needed for the calculation of the magnetic properties. Both magnetic data and theoretical studies on the Dy analogue indicate that this reduced lanthanide complex contains noninteracting Dy centers, and instead, the two centers are described as interacting with the σ-bonding electron. The complexity of the data in the Cp^{An} metallocene system contrasts with the mono-cyclopentadienyl $[(C_5{}^iPr_5)Ln]_2(\mu\text{-}I)_3$[47] complexes. The differences may arise due to different metallocene environments or the identity of the bridging atoms. Clearly, the *ansa*-metallocene environment also brings in additional factors which change the nature of this bimetallic system while delivering the shortest Y···Y distance identified to date.

ASSOCIATED CONTENT

Supporting Information

The Supporting Information is available free of charge at https://pubs.acs.org/doi/10.1021/jacs.3c01405.

Experimental details including improvement on the synthesis of **1**; χT vs T profile for the Dy^{II}−Lu^{III} model with various coupling parameters J; magnetic hysteresis data for **5** collected at 2 K; in-phase and out-of-phase components of the ac magnetic susceptibility for **5**; solid-state EPR spectrum of **4**; and UV−visible spectra of **4** in THF; and computational details (PDF)

Accession Codes

CCDC 2219700−2219705 contain the supplementary crystallographic data for this paper. These data can be obtained free of charge via www.ccdc.cam.ac.uk/data_request/cif, or by emailing data_request@ccdc.cam.ac.uk, or by contacting The Cambridge Crystallographic Data Centre, 12 Union Road, Cambridge CB2 1EZ, UK; fax: +44 1223 336033.

AUTHOR INFORMATION

Corresponding Author

William J. Evans − *Department of Chemistry, University of California, Irvine, California 92697, United States;* orcid.org/0000-0002-0651-418X; Email: wevans@uci.edu

https://doi.org/10.1021/jacs.3c01405
J. Am. Chem. Soc. 2023, 145, 10730−10742

Authors

Justin C. Wedal − *Department of Chemistry, University of California, Irvine, California 92697, United States;* orcid.org/0000-0003-0437-8601

Lauren M. Anderson-Sanchez − *Department of Chemistry, University of California, Irvine, California 92697, United States;* orcid.org/0000-0002-9697-8008

Megan T. Dumas − *Department of Chemistry, University of California, Irvine, California 92697, United States;* orcid.org/0000-0001-7000-2130

Colin A. Gould − *Department of Chemistry, University of California, Berkeley, California 94720, United States*

María J. Beltrán-Leiva − *Department of Chemistry and Biochemistry, Florida State University, Tallahassee, Florida 32306, United States;* Present Address: Theoretical Division, Los Alamos National Laboratory, Los Alamos, New Mexico 87545, United States; orcid.org/0000-0003-3221-3118

Cristian Celis-Barros − *Department of Chemistry and Biochemistry, Florida State University, Tallahassee, Florida 32306, United States;* orcid.org/0000-0002-4685-5229

Dayán Páez-Hernández − *Center of Applied Nanoscience (CANS), Universidad Andres Bello, Santiago 8370146, Chile*

Joseph W. Ziller − *Department of Chemistry, University of California, Irvine, California 92697, United States;* orcid.org/0000-0001-7404-950X

Jeffrey R. Long − *Department of Chemistry, University of California, Berkeley, California 94720, United States; Materials Sciences Division, Lawrence Berkeley National Laboratory, Berkeley, California 94720, United States; Department of Chemical and Biomolecular Engineering, University of California, Berkeley, California 94720, United States;* orcid.org/0000-0002-5324-1321

Complete contact information is available at: https://pubs.acs.org/10.1021/jacs.3c01405

Author Contributions

[▽]J.C.W. and L.M.A.-S. contributed equally, and both have the right to place their name first.

Notes

The authors declare no competing financial interest.

■ ACKNOWLEDGMENTS

The authors thank the U.S. National Science Foundation for support of this research (CHE-2154255 to W.J.E. and CHE-2102603 to J.R.L.) and FONDECYT 1180017. Furthermore, M.J.B.-L. acknowledges CONICYT/Doctorado Nacional 2015/21151553 for the Ph.D. fellowship. The authors also thank Austin J. Ryan and Daniel N. Huh for help with X-ray crystallography and UC Irvine's Laser Facility and Professors A. S. Borovik and Jenny Yang for assistance with EPR and IR spectroscopy.

■ REFERENCES

(1) Matignon, C.; Cazes, E. Un Nouveau Type de Compose dans le Group des Metaux Rares. *C. R. Acad. Sci.* **1906**, *142*, 83−85.

(2) Urbain, G.; Bourion, F. Metaux Rares. Sur le Chlorure Eurpoeux. *C. R. Acad. Sci.* **1911**, *153*, 1155−1158.

(3) Fischer, E. O.; Fischer, H. Dicyclopentadienyleuropium. *Angew. Chem., Int. Ed.* **1964**, *3*, 132−133.

(4) Klemm, W.; Schüth, W. Messungen an Zwei- und Vierwertigen Verbindungen der Seltenen Erden. III. Ytterbiumdichlorid. *Z. Anorg. Allg. Chem.* **1929**, *184*, 352−358.

(5) Fischer, E. O.; Fischer, H. Uber Dicyclopentadienyleuropium und Dicyclopentadienylytterbium und Tricyclopentadienyle des Terbiums, Holmiums, Thuliums und Lutetiums. *J. Organomet. Chem.* **1965**, *3*, 181−187.

(6) Zinnen, H. A.; Pluth, J. J.; Evans, W. J. X-Ray Crystallographic Determination of the Structure of Bis(Methyl-Cyclopentadienyl) Ytterbium Tetrahydrofuranate and Its Ready Formation by Four New Routes. *J. Chem. Soc., Chem. Commun.* **1980**, 810−812.

(7) Matignon, C.; Sazes, E. Le Chlorure Samareux. *Ann. Chim. Phys.* **1906**, *8*, 417−426.

(8) Evans, W. J.; Bloom, I.; Hunter, W. E.; Atwood, J. L. Synthesis and X-Ray Crystal Structure of a Soluble Divalent Organosamarium Complex. *J. Am. Chem. Soc.* **1981**, *103*, 6507−6508.

(9) Meyer, G. Reduced Halides of the Rare-Earth Elements. *Chem. Rev.* **1988**, *88*, 93−107.

(10) Kamenskaya, A. N.; Mikheev, N. B.; Spytsin, V. I. Complex Compounds of Bivalent Samarium and Thulium with Crown Ethers. *Dokl. Akad. Nauk SSSR* **1984**, *275*, 913−916.

(11) Bochkarev, M. N.; Fedushkin, I. L.; Fagin, A. A.; Petrovskaya, T. V.; Ziller, J. W.; Broomhall-Dillard, R. N. R.; Evans, W. J. Synthesis and Structure of the First Molecular Thulium(II) Complex: $[TmI_2(MeOCH_2CH_2OMe)_2]$. *Angew. Chem., Int. Ed.* **1997**, *36*, 133−135.

(12) Bochkarev, M. N.; Fagin, A. A. First Molecular Iodides of Neodymium(II) and Dysprosium(II). *Russ. Chem. Bull.* **1999**, *48*, 1187−1188.

(13) Bochkarev, M. N.; Fagin, A. A. A New Route to Neodymium-(II) and Dysprosium(II) Iodides. *Chem. - Eur. J.* **1999**, *5*, 2990−2992.

(14) Evans, W. J.; Allen, N. T.; Ziller, J. W. The Availability of Dysprosium Diiodide as a Powerful Reducing Agent in Organic Synthesis: Reactivity Studies and Structural Analysis of $DyI_2(DME)_3$ and Its Naphthalene Reduction Product. *J. Am. Chem. Soc.* **2000**, *122*, 11749−11750.

(15) Jaroschik, F.; Nief, F.; Le Goff, X.-F.; Ricard, L. Isolation of Stable Organodysprosium(II) Complexes by Chemical Reduction of Dysprosium(III) Precursors. *Organometallics* **2007**, *26*, 1123−1125.

(16) Bochkarev, M. N.; Fedushkin, I. L.; Dechert, S.; Fagin, A. A.; Schumann, H. $[NdI_2(Thf)_5]$, the First Crystallographically Authenticated Neodymium(II) Complex. *Angew. Chem., Int. Ed.* **2001**, *40*, 3176−3178.

(17) Bochkarev, M. N. Molecular Compounds of "New" Divalent Lanthanides. *Coord. Chem. Rev.* **2004**, *248*, 835−851.

(18) Meyer, G. The Divalent State in Solid Rare-Earth Metal Haldes. In *The Rare Earth Elements: Fundamentals and Applications*; Atwood, D. A., Ed.; Wiley: New York, 2012; pp 241−300.

(19) Nief, F. Molecular Chemistry of the Rare-Earth Elements in Uncommon Low-Valent States. In *Handbook on the Physics and Chemistry of Rare Earths*; Gschneidner, K. A.; Bunzil, J.-C. G.; Pecharsky, V. K., Eds.; Elsevier Science: Amsterdam, 2010; pp 241−300.

(20) Hitchcock, P. B.; Lappert, M. F.; Maron, L.; Protchenko, A. V. Lanthanum Does Form Stable Molecular Compounds in the +2 Oxidation State. *Angew. Chem., Int. Ed.* **2008**, *47*, 1488−1491.

(21) MacDonald, M. R.; Bates, J. E.; Ziller, J. W.; Furche, F.; Evans, W. J. Completing the Series of +2 Ions for the Lanthanide Elements: Synthesis of Molecular Complexes of Pr^{2+}, Gd^{2+}, Tb^{2+}, and Lu^{2+}. *J. Am. Chem. Soc.* **2013**, *135*, 9857−9868.

(22) MacDonald, M. R.; Bates, J. E.; Fieser, M. E.; Ziller, J. W.; Furche, F.; Evans, W. J. Expanding Rare-Earth Oxidation State Chemistry to Molecular Complexes of Holmium(II) and Erbium(II). *J. Am. Chem. Soc.* **2012**, *134*, 8420−8423.

(23) MacDonald, M. R.; Ziller, J. W.; Evans, W. J. Synthesis of a Crystalline Molecular Complex of Y^{2+}, $[(18\text{-Crown-6})K][(C_5H_4SiMe_3)_3Y]$. *J. Am. Chem. Soc.* **2011**, *133*, 15914−15917.

(24) Evans, W. J. Tutorial on the Role of Cyclopentadienyl Ligands in the Discovery of Molecular Complexes of the Rare-Earth and Actinide Metals in New Oxidation States. *Organometallics* **2016**, *35*, 3088−3100.

(25) Woen, D. H.; Evans, W. J. Expanding the +2 Oxidation State of the Rare-Earth Metals, Uranium, and Thorium in Molecular Complexes. In *Handbook on the Physics and Chemistry of Rare Earths*; Bünzli, J.-C.; Pecharsky, V. K., Eds.; Elsevier B.V., 2016; pp 337−394.
(26) Wedal, J. C.; Evans, W. J. A Rare-Earth Metal Retrospective to Stimulate All Fields. *J. Am. Chem. Soc.* **2021**, *143*, 18354−18367.
(27) Trinh, M. T.; Wedal, J. C.; Evans, W. J. Evaluating Electrochemical Accessibility of $4f^n5d^1$ and $4f^{n+1}$ Ln(II) Ions in $(C_5H_4SiMe_3)_3Ln$ and $(C_5Me_4H)_3Ln$ Complexes. *Dalton Trans.* **2021**, *50*, 14384−14389.
(28) Fieser, M. E.; MacDonald, M. R.; Krull, B. T.; Bates, J. E.; Ziller, J. W.; Furche, F.; Evans, W. J. Structural, Spectroscopic, and Theoretical Comparison of Traditional vs Recently Discovered Ln^{2+} Ions in the $[K(2.2.2\text{-Cryptand})][(C_5H_4SiMe_3)_3Ln]$ Complexes: The Variable Nature of Dy^{2+} and Nd^{2+}. *J. Am. Chem. Soc.* **2015**, *137*, 369−382.
(29) Meihaus, K. R.; Fieser, M. E.; Corbey, J. F.; Evans, W. J.; Long, J. R. Record High Single-Ion Magnetic Moments Through $4f^n5d^1$ Electron Configurations in the Divalent Lanthanide Complexes $[(C_5H_4SiMe_3)_3Ln]^-$. *J. Am. Chem. Soc.* **2015**, *137*, 9855−9860.
(30) Palumbo, C. T.; Darago, L. E.; Windorff, C. J.; Ziller, J. W.; Evans, W. J. Trimethylsilyl versus Bis(Trimethylsilyl) Substitution in Tris(Cyclopentadienyl) Complexes of La, Ce, and Pr: Comparison of Structure, Magnetic Properties, and Reactivity. *Organometallics* **2018**, *37*, 900−905.
(31) Seitz, M.; Oliver, A. G.; Raymond, K. N. The Lanthanide Contraction Revisited. *J. Am. Chem. Soc.* **2007**, *129*, 11153−11160.
(32) Crosswhite, H. M.; Crosswhite, H.; Carnall, W. T.; Paszek, A. P. Spectrum Analysis of U^{3+}:$LaCl_3$. *J. Chem. Phys.* **1980**, *72*, 5103−5117.
(33) Atwood, D. *The Rare Earth Elements: Fundamentals and Applications*; John Wiley & Sons, 2012.
(34) Pan, C.; Shen, W.; Yang, L.; Bao, L.; Wei, Z.; Jin, P.; Fang, H.; Xie, Y.; Akasaka, T.; Lu, X. Crystallographic Characterization of Y_2C_{2n} (2n = 82, 88−94): Direct Y−Y Bonding and Cage-Dependent Cluster Evolution. *Chem. Sci.* **2019**, *10*, 4707−4713.
(35) Yang, T.; Zhao, X.; Osawa, E. Can a Metal-Metal Bond Hop in the Fullerene Cage? *Chem. - Eur. J.* **2011**, *17*, 10230−10234.
(36) Popov, A. A.; Avdoshenko, S. M.; Pendás, A. M.; Dunsch, L. Bonding between Strongly Repulsive Metal Atoms: An Oxymoron Made Real in a Confined Space of Endohedral Metallofullerenes. *Chem. Commun.* **2012**, *48*, 8031−8050.
(37) Zuo, T.; Xu, L.; Beavers, C. M.; Olmstead, M. M.; Fu, W.; Crawford, T. D.; Balch, A. L.; Dorn, H. C. $M_2@C_{79}N$ (M = Y, Tb): Isolation and Characterization of Stable Endohedral Metallofullerenes Exhibiting M−M Bonding Interactions inside Aza[80]Fullerene Cages. *J. Am. Chem. Soc.* **2008**, *130*, 12992−12997.
(38) Bao, L.; Chen, M.; Pan, C.; Yamaguchi, T.; Kato, T.; Olmstead, M. M.; Balch, A. L.; Akasaka, T.; Lu, X. Crystallographic Evidence for Direct Metal-Metal Bonding in a Stable Open-Shell $La_2@I_h$-C_{80} Derivative. *Angew. Chem., Int. Ed.* **2016**, *55*, 4242−4246.
(39) Yamada, M.; Kurihara, H.; Suzuki, M.; Saito, M.; Slanina, Z.; Uhlik, F.; Aizawa, T.; Kato, T.; Olmstead, M. M.; Balch, A. L.; Maeda, Y.; Nagase, S.; Lu, X.; Akasaka, T. Hiding and Recovering Electrons in a Dimetallic Endohedral Fullerene: Air-Stable Products from Radical Additions. *J. Am. Chem. Soc.* **2015**, *137*, 232−238.
(40) Liu, F.; Krylov, D. S.; Spree, L.; Avdoshenko, S. M.; Samoylova, N. A.; Rosenkranz, M.; Kostanyan, A.; Greber, T.; Wolter, A. U. B.; Büchner, B.; Popov, A. A. Single Molecule Magnet with an Unpaired Electron Trapped between Two Lanthanide Ions inside a Fullerene. *Nat. Commun.* **2017**, *8*, 16098.
(41) Shen, W.; Bao, L.; Wu, Y.; Pan, C.; Zhao, S.; Fang, H.; Xie, Y.; Jin, P.; Peng, P.; Li, F.-F.; Lu, X. $Lu_2@C_{2n}$ (2n = 82, 84, 86): Crystallographic Evidence of Direct Lu−Lu Bonding between Two Divalent Lutetium Ions Inside Fullerene Cages. *J. Am. Chem. Soc.* **2017**, *139*, 9979−9984.
(42) Dumas, M. T.; Chen, G. P.; Hu, J. Y.; Nascimento, M. A.; Rawson, J. M.; Ziller, J. W.; Furche, F.; Evans, W. J. Synthesis and Reductive Chemistry of Bimetallic and Trimetallic Rare-Earth Metallocene Hydrides with $(C_5H_4SiMe_3)^{1-}$ Ligands. *J. Organomet. Chem.* **2017**, *849*−*850*, 38−47.
(43) Ortiz, J. V.; Hoffmann, R. Hydride Bridges between $LnCp_2$ Centers. *Inorg. Chem.* **1985**, *24*, 2095−2104.
(44) Venanzi, L. M. Transition Metal Complexes With Bridging Hydride Ligands. *Coord. Chem. Rev.* **1982**, *43*, 251−274.
(45) Dumas, M. T.; Ziller, J. W.; Evans, W. J. Synthesis and Reduction of Bimetallic Methyl-Bridged Rare-Earth Metal Complexes, $[(C_5H_4SiMe_3)_2Ln(\mu\text{-}CH_3)]_2$ (Ln = Y, Tb, Dy). *ACS Omega* **2019**, *4*, 398−402.
(46) Desurmont, G.; Li, Y.; Yasuda, H.; Maruo, T.; Kanehisa, N.; Kai, Y. Reaction Pathway for the Formation of Binuclear Samarocene Hydride from Monomeric Alkyl Samarocene Derivative and the Effective Catalysis of Samarocene Hydride for the Block Copolymerization of Ethylene with Polar Monomers. *Organometallics* **2000**, *19*, 1811−1813.
(47) Gould, C. A.; McClain, K. R.; Reta, D.; Kragskow, J. G. C.; Marchiori, D. A.; Lachman, E.; Choi, E.; Analytis, J. G.; Britt, R. D.; Chilton, N. F.; Harvey, B. G.; Long, J. R. Ultrahard Magnetism from Mixed-Valence Dilanthanide Complexes with Metal−Metal Bonding. *Science* **2022**, *375*, 198−202.
(48) McClain, K. R.; Gould, C. A.; Marchiori, D. A.; Kwon, H.; Nguyen, T. T.; Rosenkoetter, K. E.; Kuzmina, D.; Tuna, F.; Britt, R. D.; Long, J. R.; Harvey, B. G. Divalent Lanthanide Metallocene Complexes with a Linear Coordination Geometry and Pronounced 6s−5d Orbital Mixing. *J. Am. Chem. Soc.* **2022**, *144*, 22193−22201.
(49) Molander, G. A.; Dowdy, E. D.; Schumann, H. Catalytic Cyclization/Silylation of Dienes Containing 1,1-Disubstituted Olefins Using Organolanthanide and Group 3 Organometallic Complexes. *J. Org. Chem.* **1998**, *63*, 3386−3396.
(50) Khvostov, A. V.; Belsky, V. K.; Bulychev, B. M.; Sizov, A. I.; Ustinov, B. B. Ansa-Ytterbocenes(+3) with a Short Bridge and Bulky Substituents: Synthesis and Crystal Structure of *meso*-$(CH_3)_2Si[3\text{-}(CH_3)_3SiC_5H_3]_2YbCl(THF)$, *rac*-$(CH_3)_2C[3\text{-}^tBuC_5H_3]_2Yb(\mu^2\text{-}Cl)_2Li(OEt_2)_2$, and $[meso\text{-}(CH_3)_2C[3\text{-}^tBuC_5H_3]_2Yb[\mu^2\text{-}OCH_3)]_2$. *J. Organomet. Chem.* **1998**, *571*, 243−249.
(51) Evans, W. J.; Kozimor, S. A.; Brady, J. C.; Davis, B. L.; Nyce, G. W.; Seibel, C. A.; Ziller, J. W.; Doedens, R. J. Metallocene Allyl Reactivity in the Presence of Alkenes Tethered to Cyclopentadienyl Ligands. *Organometallics* **2005**, *24*, 2269−2278.
(52) Evans, W. J.; Meadows, J. H.; Wayda, A. L.; Hunter, W. E.; Atwood, J. L. Organolanthanide Hydride Chemistry. 1. Synthesis and X-Ray Crystallographic Characterization of Dimeric Organolanthanide and Organoyttrium Hydride Complexes. *J. Am. Chem. Soc.* **1982**, *104*, 2008−2014.
(53) Evans, W. J.; Drummond, D. K.; Hanusa, T. P.; Doedens, R. J. Organolanthanide and Organoyttrium Hydride Chemistry. 9. Bis(1,3-Dimethylcyclopentadienyl)Yttrium Complexes. Synthesis and X-Ray Crystallographic Characterization of $[(1,3\text{-}Me_2C_5H_3)_2Y(\mu\text{-}Me)]_2$, $[(1,3\text{-}Me_2C_5H_3)_2Y(\mu\text{-}H)]_3$, and $[(1,3\text{-}Me_2C_5H_3)_2(THF)Y(\mu\text{-}H)]_2$. *Organometallics* **1987**, *6*, 2279−2285.
(54) Zhang, J.; Yi, W.; Zhang, Z.; Chen, Z.; Zhou, X. Facile Synthesis of Organolanthanide Hydrides with Metallic Potassium: Crystal Structures and Reactivity. *Organometallics* **2011**, *30*, 4320−4324.
(55) Arndt, S.; Kramer, M. U.; Fegler, W.; Nakajima, Y.; Del Rosal, I.; Poteau, R.; Spaniol, T. P.; Maron, L.; Okuda, J. Yttrium Dihydride Cation $[YH_2(THF)_2]_n^+$: Aggregate Formation and Reaction with (NNNN)-Type Macrocycles. *Organometallics* **2015**, *34*, 3739−3747.
(56) Gountchev, T. I.; Tilley, T. D. Yttrium Complexes of the Chelating, C_2-Symmetric, Bis(Silylamido)Biphenyl Ligand $[DADMB]^{2-}$ $(=\{[6,6'\text{-}Me_2\text{-}(C_6H_3)_2](2,2'\text{-}NSiMe_2{}^tBu)_2\}^{2-})$. *Organometallics* **1999**, *18*, 2896−2905.
(57) Hultzsch, K. C.; Spaniol, T. P.; Okuda, J. Half-Sandwich Alkyl and Hydrido Complexes of Yttrium: Convenient Synthesis and Polymerization Catalysis of Polar Monomers. *Angew. Chem., Int. Ed.* **1999**, *38*, 227−230.
(58) Trifonov, A. A.; Skvortsov, G. G.; Lyubov, D. M.; Skorodumova, N. A.; Fukin, G. K.; Baranov, E. V.; Glushakova, V.

https://doi.org/10.1021/jacs.3c01405
J. Am. Chem. Soc. 2023, 145, 10730−10742

N. Postmetallocene Lanthanide−Hydrido Chemistry: A New Family of Complexes [{Ln{(Me$_3$Si)$_2$NC(N^{i}Pr)$_2$}$_2$(μ-H)}$_2$] (Ln=Y, Nd, Sm, Gd, Yb) Supported by Guanidinate Ligands—Synthesis, Structure, and Catalytic Activity in Olefin Polymerization. *Chem. - Eur. J.* **2006**, *12*, 5320−5327.
(59) Corbey, J. F.; Woen, D. H.; Palumbo, C. T.; Fieser, M. E.; Ziller, J. W.; Furche, F.; Evans, W. J. Ligand Effects in the Synthesis of Ln^{2+} Complexes by Reduction of Tris(Cyclopentadienyl) Precursors Including C−H Bond Activation of an Indenyl Anion. *Organometallics* **2015**, *34*, 3909−3921.
(60) Fang, M.; Bates, J. E.; Lorenz, S. E.; Lee, D. S.; Rego, D. B.; Ziller, J. W.; Furche, F.; Evans, W. J. $(N_2)^{3-}$ Radical Chemistry via Trivalent Lanthanide Salt/Alkali Metal Reduction of Dinitrogen: New Syntheses and Examples of $(N_2)^{2-}$ and $(N_2)^{3-}$ Complexes and Density Functional Theory Comparisons of Closed Shell Sc^{3+}, Y^{3+}, and Lu^{3+} versus $4f^9$ Dy^{3+}. *Inorg. Chem.* **2011**, *50*, 1459−1469.
(61) Moehring, S. A.; Miehlich, M.; Hoerger, C. J.; Meyer, K.; Ziller, J. W.; Evans, W. J. A Room-Temperature Stable Y(II) Aryloxide: Using Steric Saturation to Kinetically Stabilize Y(II) Complexes. *Inorg. Chem.* **2020**, *59*, 3207−3214.
(62) Moehring, S. A.; Evans, W. J. Evaluating Electron Transfer Reactivity of Rare-Earth Metal(II) Complexes Using EPR Spectroscopy. *Organometallics* **2020**, *39*, 1187−1194.
(63) Kundu, K.; White, J. R. K.; Moehring, S. A.; Yu, J. M.; Ziller, J. W.; Furche, F.; Evans, W. J.; Hill, S. A 9.2-GHz Clock Transition in a Lu(II) Molecular Spin Qubit Arising from a 3,467-MHz Hyperfine Interaction. *Nat. Chem.* **2022**, *14*, 392−397.
(64) Reed, A. E.; Weinhold, F. Natural Localized Molecular Orbitals. *J. Chem. Phys.* **1985**, *83*, 1736−1740.
(65) Parthey, M.; Kaupp, M. Quantum-Chemical Insights into Mixed-Valence Systems: Within and beyond the Robin−Day Scheme. *Chem. Soc. Rev.* **2014**, *43*, 5067−5088.
(66) Bursten, B. E.; Rhodes, L. F.; Strittmatter, R. J. Bonding in Tris(η^5-Cyclopentadienyl) Actinide Complexes. 2. On the Ground Electronic Configurations of "Base-Free" Cp_3An Complexes (An = Th, Pa, U, Np, Pu). *J. Am. Chem. Soc.* **1989**, *111*, 2756−2758.
(67) *Molecular Metal-Metal Bonds: Compounds, Synthesis, Properties*; Liddle, S. T., Ed.; Wiley-VCH Verlag GmbH & Co. KGaA: Weinheim, Germany, 2015.
(68) Vahrenkamp, H. What Do We Know about the Metal-Metal Bond? *Angew. Chem., Int. Ed.* **1978**, *17*, 379−392.
(69) Nichols, J. M.; Wolf, J.; Zavalij, P.; Varughese, B.; Doyle, M. P. Bis(Phenyl)Dirhodium(III) Caprolactamate: A Dinuclear Paddlewheel Complex with No Metal−Metal Bond. *J. Am. Chem. Soc.* **2007**, *129*, 3504−3505.
(70) Zhang, Q.; Li, W.-L.; Zhao, L.; Chen, M.; Zhou, M.; Li, J.; Frenking, G. A Very Short Be-Be Distance but No Bond: Synthesis and Bonding Analysis of Ng-Be_2O_2-Ng′ (Ng, Ng′=Ne, Ar, Kr, Xe). *Chem. - Eur. J.* **2017**, *23*, 2035−2039.
(71) Robin, M. B.; Day, P. Mixed-Valent Chemistry - A Survey and Classification. In *Advances in Inorganic Chemistry and Radiochemistry*; Elsevier, 1968; pp 247−422.
(72) Demadis, K. D.; Hartshorn, C. M.; Meyer, T. J. The Localized-to-Delocalized Transition in Mixed-Valence Chemistry. *Chem. Rev.* **2001**, *101*, 2655−2686.
(73) D'Alessandro, D. M.; Keene, F. R. Current Trends and Future Challenges in the Experimental, Theoretical and Computational Analysis of Intervalence Charge Transfer (IVCT) Transitions. *Chem. Soc. Rev.* **2006**, *35*, 424−440.
(74) Brunschwig, B. S.; Creutz, C.; Sutin, N. Optical Transitions of Symmetrical Mixed-Valence Systems in the Class II-III Transition Regime. *Chem. Soc. Rev.* **2002**, *31*, 168−184.
(75) Venugopal, A.; Tuna, F.; Spaniol, T. P.; Ungur, L.; Chibotaru, L. F.; Okuda, J.; Layfield, R. A. A Hydride-Ligated Dysprosium Single-Molecule Magnet. *Chem. Commun.* **2013**, *49*, 901−903.

https://doi.org/10.1021/jacs.3c01405
J. Am. Chem. Soc. 2023, 145, 10730−10742